33rd Annual International Conference of the IEEE EMBS
Boston, Massachusetts USA, August 30 - September 3, 2011

Estimating Brain Microvascular Blood Flows from Partial Two-Photon Microscopy Data by Computation with a Circuit Model

John Sunwoo, Nathan R. Cornelius, Peter C. Doerschuk, and Chris B. Schaffer

Abstract—**The cortical microvasculature plays a key role in cortical tissue health by transporting important molecules via blood. Disruptions to blood flow in the microvasculature due to events such as stroke can thus induce damage to the cortex. Recent developments in two-photon microscopy have enabled *in vivo* imaging of anesthetized rat cortex in three dimensions. The microscopy data provide information about the geometry of the cortical microvasculature, length and diameter of the vessels in the imaged microvasculature network, and blood flow through a subset of those vessels. We demonstrate a model that achieves three goals. First, given a network of interconnected vessels and flow measurements on a subset of those vessels, we can estimate the flows in the remaining vessels. Second, we can determine which and how many vessels should have blood flow measurements taken to provide sufficient information to predict the unmeasured flows. Finally, the model enables us to predict effects of blockages in one or more vessels, indicating which vessels are most important to overall flow in the network.**

I. Introduction

THE cortical microvasculature is comprised of a complicated network of arterioles, capillaries, and venules in which blood flow transports molecules to and from the cortical tissue. Since molecular transport across the blood-brain barrier primarily occurs in the microvasculature (especially the capillaries), these vessels are crucial to the metabolism, energetics, and functionality of the cortex. Occlusions, such as small stroke, are thus damaging to cortical health as they impede microcirculation.

Two-photon excited fluorescence (2PEF) microscopy allows *in vivo* imaging of the microvasculature to depths of 1mm, as well as blood flow measurements in vessels by tracking the time-varying position of individual red blood cells. While all vessels within the microscope's imaging range (typically a 1mm^3 volume) can be resolved, blood flow measurements can be made on only a subset of these vessels due to experimental limitations, such as the practical duration of anesthesia for a rat. The goal of the research is to use computational tools to estimate the blood flows in all the vessels. A model is thus needed to relate the measured and unmeasured blood flows. Inputs to the model are vessel diameter, length, interconnection topology, and the measured blood flows. The output of the model is predictions for flow velocity in every imaged vessel.

Manuscript received April 15, 2011. This work was supported in part by Sandia National Laboratories LRD 11-0954 (SNL 1105).

The authors are with the Cornell University Department of Biomedical Engineering, Ithaca, NY 14850

II. Methods and Materials

Methods for the two-photon microscopy data acquisition on anesthetized rats are described in [1]. We model the microvasculature as a resistive circuit in which current, q, is blood flow, and voltage, V, is blood pressure. Each vessel in the network represents a resistive branch that connects two nodes, or vessel bifurcation points, in the microvasculature. The circuit obeys Kirchhoff's current law (KCL), Kirchhoff's voltage law (KVL), and Ohm's law so that current is conserved at nodes and the voltage drop across a branch is proportional to the current through the branch and the branch's resistance. The resistance, R, of each branch is computed using Poiseuille's Law, assuming that the vessel is straight, which describes a relationship between length, l, radius, a, and blood viscosity, η, for nonturbulent flow. The formula is

$$R(l,\eta,a)=\frac{8\eta \mathrm{l}}{\pi a^4}. \quad (1)$$

In reality blood exhibits non-Newtonian flow characteristics because of its slurry-like composition of cells and plasma. To correct for non-Newtonian effects we use a diameter-dependent viscosity, $\eta(d)$, described by [2], [3]. As shown in Fig. 6 of [2], the viscosity at hematocrit 45% varies by a factor of three over the range of vessel diameters greater than 10μm.

The microvasculature extends outside of the volume of brain that is imaged. Therefore there are branches of the circuit that connect a node within the image to a node outside the image, and thus the circuit is incomplete. We complete the circuit by placing a voltage source at each cut branch. We refer to these voltages as boundary voltages. We use a voltage source rather than a current source because the heart is more nearly a voltage source. One of the boundary voltages is arbitrarily set to zero to represent a ground node. Because of the many cut branches (30, shown in Fig. 2A), the circuit has many input and many output nodes. Vessel bifurcations where vessels split or join are called internal nodes. Voltages at these nodes are called internal voltages. Fig. 1a and Fig. 1b show a small scale example of an imaged microvasculature topology and its corresponding circuit model, respectively. Typical flows (μL/s) are shown in Fig. 2A.

Let I_n be the $n \times n$ identity matrix. Let N_{in} be the number of internal nodes and N_{bnd} be the number of

boundary nodes. Let positive integers $i,j \in \{1,\ldots,N_{in}+N_{bnd}\}$ index the nodes. Let indexes $\{1,\ldots,N_{in}\}$ represent internal nodes, let indexes $\{N_{in}+1,\ldots, N_{in}+N_{bnd}-1\}$ represent boundary nodes where the boundary voltage sources are placed, and let index $N_{in} + N_{bnd}$ represent the ground node.

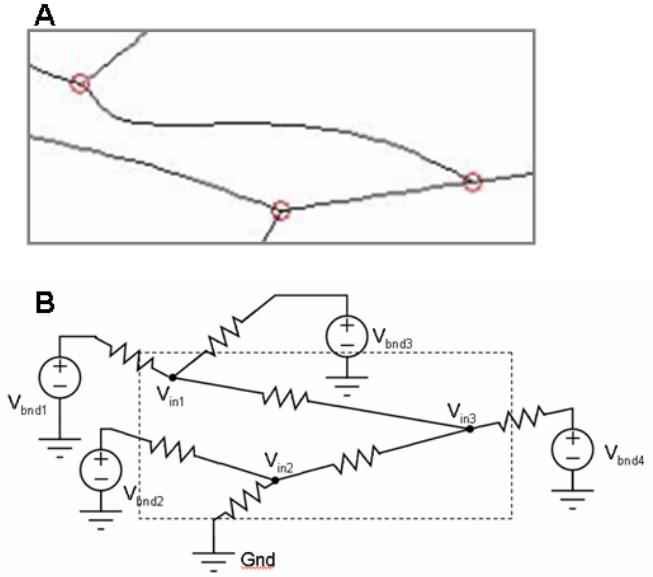

Fig. 1. A small-scale example of a vessel topology with three internal nodes and five cut branches is shown in (a). The corresponding circuit model with voltage sources attached to the cut branches is shown in (b).

For simplicity in the equations, it is assumed that every pair of internal nodes is connected, with $R_{i,j}=R_{j,i}>0$. Currents between nodes are represented by $q_{i,j}$, where $q_{i,j}= -q_{j,i}$. Branches between nodes in our model that do not exist in the microvasculature will have resistance value of infinity. Thus current in these branches is zero, which in effect represents the absence of a connection between these nodes. Let the voltages at node i be denoted V_i. Define internal voltages, $V_{in}=(V_1,\ldots,V_{Nin})^T$, boundary voltages $V_{bnd}=(V_{Nin+1},\ldots,V_{Nin+Nbnd-1})^T$, and ground voltage $V_g=(V_{Nin+Nbnd})$. The vector containing both internal and boundary voltages (but not ground) is defined as $V=(V_{in}{}^T, V_{bnd}{}^T)^T$. The choice of the definition of ground has no effect on the results because the measurements are exclusively currents which depend solely on voltage differences.

At each of the N_{in} internal nodes, write KCL, i.e., the sum of the currents entering (or leaving) the node is zero. For $n \in \{1,\ldots,N_{in}\}$, the form of the equations is

$$\sum_{m=1,m\neq n}^{N_{in}+N_{bnd}} \frac{V_n - V_m}{R_{n,m}} = 0, \tag{2}$$

which is equivalent to

$$V_n \sum_{m=1,m\neq n}^{N_{in}+N_{bnd}} \frac{1}{R_{n,m}} - \sum_{m=1,m\neq n}^{N_{in}+N_{bnd}} \frac{V_m}{R_{n,m}} = 0. \tag{3}$$

Subdivide the second sum to get

$$V_n \sum_{m=1,m\neq n}^{N_{in}+N_{bnd}} \frac{1}{R_{n,m}} - \left(\sum_{m=1,m\neq n}^{N_{in}} \frac{V_m}{R_{n,m}} + \sum_{m=N_{in}+1}^{N_{in}+N_{bnd}-1} \frac{V_m}{R_{n,m}} + \frac{V_{N_{in}+N_{bnd}}}{R_{n,N_{in}+N_{bnd}}} \right) = 0. \tag{4}$$

Use the fact that $V_{N_{in}+N_{bnd}} = 0$ since it is ground to get

$$V_n \sum_{m=1,m\neq n}^{N_{in}+N_{bnd}} \frac{1}{R_{n,m}} - \left(\sum_{m=1,m\neq n}^{N_{in}} \frac{V_m}{R_{n,m}} + \sum_{m=N_{in}+1}^{N_{in}+N_{bnd}-1} \frac{V_m}{R_{n,m}} \right) = 0. \tag{5}$$

Move terms that involve the boundary condition voltage sources to the right hand side of the equations to get

$$V_n \sum_{m=1,m\neq n}^{N_{in}+N_{bnd}} \frac{1}{R_{n,m}} - \sum_{m=1,m\neq n}^{N_{in}} \frac{V_m}{R_{n,m}} = \sum_{m=N_{in}+1}^{N_{in}+N_{bnd}-1} \frac{V_m}{R_{n,m}}. \tag{6}$$

Define two matrices of conductances, denoted by $G \in \Re^{N_{in}\times N_{in}}$ and $B \in \Re^{N_{in}\times(N_{bnd}-1)}$, by

$$G_{n,m} = \begin{cases} -\sum_{m=1,m\neq n}^{N_{in}+N_{bnd}} \frac{1}{R_{n,m}}, n = m \\ \frac{1}{R_{n,m}}, n \neq m \end{cases} \tag{7}$$

$$B_{n,m} = -\frac{1}{R_{n,m}}. \tag{8}$$

The negative of (7) can be written in the form

$$GV_{in} = BV_{bnd} \tag{9}$$

which implies

$$V_{in} = G^{-1}BV_{bnd}. \tag{10}$$

Finally,

$$V = \begin{bmatrix} V_{in} \\ V_{bnd} \end{bmatrix} = \begin{bmatrix} G^{-1}B \\ I_{N_{bnd}-1} \end{bmatrix} V_{bnd}. \tag{11}$$

All currents can be computed by

$$q_{i,j} = \frac{V_i - V_j}{R_{i,j}}. \tag{12}$$

Let $\alpha=(i,j)$, for $(i,j \in \xi=\{1,\ldots,N_{in}+N_{bnd}\})$, be an index describing a flow by giving the nodes at either end of the branch. Let $i=\varphi(\alpha)$ and $j=\psi(\alpha)$ be the node indices. Let $q^{(\xi)} = (q_{\phi(1),\psi(1)},\ldots,q_{\phi(N_\xi),\psi(N\varsigma)})$ be a vector whose elements are the flows. Define $C \in \Re^{N_\xi \times N_{bnd}}$ with components $C_{\alpha,n}$ by

$$C_{\alpha,n} = \begin{cases} 1/R_{\phi(\alpha),\psi(\alpha)} & n = \phi(\alpha) \\ -1/R_{\phi(\alpha),\psi(\alpha)} & n = \psi(\alpha) \\ 0 & otherwise. \end{cases} \quad (13)$$

Then

$$q^{(\xi)} = CV = C\begin{bmatrix} G^{-1}B \\ I_{N_{bnd}-1} \end{bmatrix} V_{bnd} = L^{\xi} V_{bnd} \quad (14)$$

where $L \in \Re^{N_\xi \times N_{bnd}}$ is defined by

$$L^{\xi} = C\begin{bmatrix} G^{-1}B \\ I_{N_{bnd}-1} \end{bmatrix}. \quad (15)$$

We use a least squares approach to predict the boundary voltages as a function of measured currents. Specifically,

$$\hat{V}_{bnd}(\xi) = \arg\min_{V_{bnd}} \left\| q^{(measured,\xi)} - q^{(\xi)}(V_{bnd}) \right\|_2^2. \quad (16)$$

If the problem is underdetermined, then there are many V_{bnd} that exactly achieve the global minimum of

$$\left\| q^{(measured,\xi)} - q^{(\xi)}(V_{bnd}) \right\|_2^2. \quad (17)$$

We take the particular V_{bnd} solution that has the minimum Euclidean norm.

III. Results

An example of a neurovascular network is shown in Fig. 2. It contains 66 vessel branches, of which 44 currents are measured. The branches with measured currents are marked in red in (a). All vessel lengths and diameters are also measured, which are qualitatively shown in (b). Two larger vessels run mostly horizontally across the top and bottom of the image, with smaller vessels between them. Measured vessel diameters range from 2.93-46.23µm. The network contains 34 vessel bifurcations, which represent 34 internal nodes in our model. The number of cut branches is 30. Therefore in our model we have 30 boundary voltage sources, one of which is set to 0V to represent the ground node. As a function of the current connection topology and number and location of measurements, these least square problems can have non-unique global minima, specifically a unique vector plus any vector lying in a subspace. Among these solutions, we pick the minimum Euclidean norm solution which is provided by the Moore-Penrose pseudoinverse which we compute with singular values in Matlab. In the particular case of Fig. 2, the rank deficiency is 5.

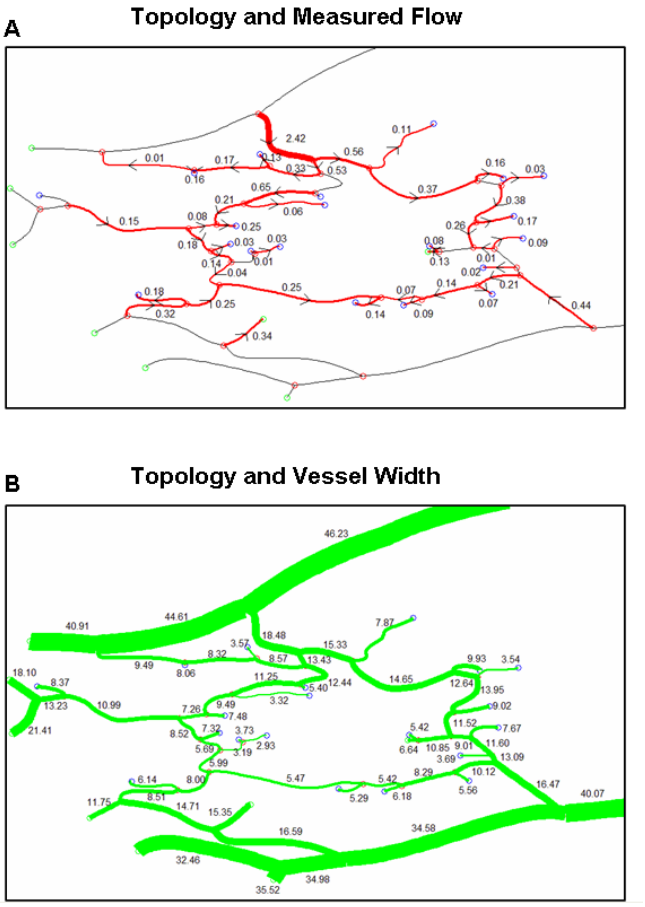

Fig. 2. The same vessel topology with 66 branches is shown in (a) and (b). (a) shows in red the 44 vessels where flow is measured. The vessels where no measurements are taken are shown in black. (b) shows vessel diameters relative to the other vessels in the image. Flow in µL/s. Diameter in µm.

Fig. 3 shows the complete set of currents estimated from the least squares problem. The magnitude of the predicted flow velocity is proportional to the thickness of the drawn vessels. Three of our predicted currents flow in the reverse direction of their corresponding measured currents. To summarize the performance of the least squares problem, the ratio of the sum of the squared error to the sum of the squared data measurements,

$$r = \frac{\sum_{j=1}^{44} (q_j^{measured} - \hat{q}_j)^2}{\sum_{j=1}^{44} (q_j^{measured})^2}, \quad (18)$$

is 0.8396/8.3360=0.1004. Reasons for r to not be smaller include the change in the animal's physiology during the two plus hour experiment and the constraints implied by KCL and KVL.

To assess the performance as a function of the number of measurements taken, we sequentially omit measurements at random, and calculate the resulting error after each omission. The high number of permutations of omission sequences prevents us from computing errors for all sequences, but a sufficient number of Monte Carlo runs give us a reasonable

understanding of the performance behavior. Fig. 4 shows statistics from 1000 of such random omitted-measurement runs. Error is computed as in (18). The median of the error contains two knees; one occurring after about 8 omitted measurements, and another after about 22.

The dynamic range of the data is large (0.004 to 2.42 μL/s) so when the flow in a large vessel is not measured and the prediction is inaccurate, the contribution to the error is much greater than the corresponding situation for a small vessel. Since there are few large vessels, different random omissions can have different numbers of such large vessels. Furthermore, at a junction of three vessels, measuring two of the vessels and applying KCL gives the entire set. This effect can ripple through the circuit since each time KCL provides a value for an unmeasured current which increases the probability that KCL at some connecting node will also provide a new current value. However, when an additional measurement is deleted leaving a node with only one measured current, KCL is not useful and the error can rise abruptly.

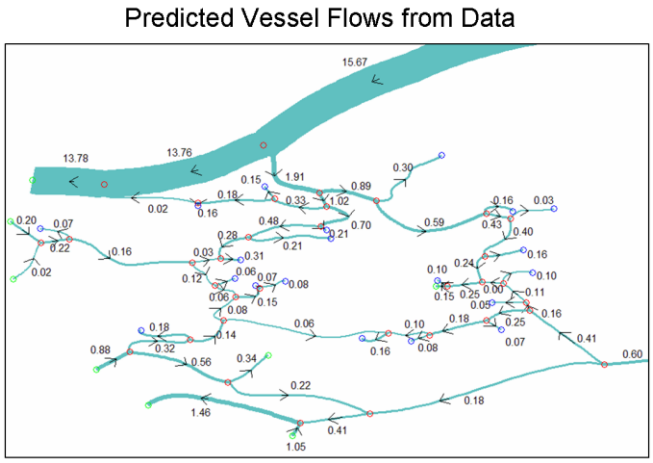

Fig. 3. The least squares solution in which all currents are estimated. Larger current magnitude estimates are depicted as wider vessels in the topology.

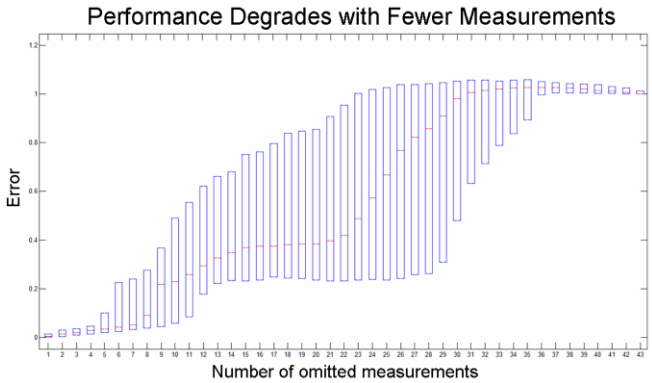

Fig. 4. Monte Carlo run statistics showing how error evolves as a greater number of measurements are left out of the least squares problem. The red mark is the median of the data. The edges of the blue box represent the 25th and 75th percentiles.

IV. Discussion and Conclusions

In this paper we present a methodology for determining a complete set of flows from a limited set of measured flows by using a linear current model and apply it to an experimental example. One attractive feature of the methodology is that multiple measurements of the same flow (possibly with variance information) can easily be incorporated. This type of information on flows in every vessel of the microvasculature and how flows adjust to obstruction has not been available in the past.

As is shown by the example in Fig. 2, the vessel network typically has many cut branches due to the complicated microvascular topology. Therefore the approach introduced in this paper, where cut branches are attached to voltage sources, is crucial for extracting flow information from these data sets. As is shown in Fig. 3, there is a wide range of flows, which is partly correlated with the wide range in vessel diameters.

Fig. 4 demonstrates that some measurements are much more important than others. Because we see that error in a Monte Carlo run typically increases monotonically with number of omitted measurements, the high variability in error in the central portion of the graph means that certain sequences of omitted measurements can result in low error for a large number of vessel omissions, while other sequences result in high error very early on. This is important for the design of experiments, since measuring certain vessels is crucial to accurately estimating the behavior of the rest of the network. A similar Monte Carlo calculation (not shown) can be done to evaluate the robustness of the network to occlusion of one or more vessels. Occlusion corresponds to a microstroke and to setting resistance in the affected branch to infinity. Quantities such as total flow into capillaries measure the robustness of the network.

As the microscopy technology advances so that the flow in a vessel can typically be measured multiple times, the model could be augmented with a temporal model which describes the evolution of the animal's neurocirculation under anesthesia which might be useful in the management of human anesthesia.

References

[1] N. Nishimura, N. Rosidi, C Iadecola, and C Schaffer, "Limitations of collateral flow after an occlusion of a single cortical penetrating arteriole," *J. Cereb Blood Flow Metab*, vol. 30, pp. 1914-1927, September 2010.

[2] A. Pries, T. Secomb, T. Gessner, M. Sperandio, J. Gross, and P. Gaehtgens, "Resistance to blood flow in microvessels in vivo," *Circ Res*, vol. 75, pp. 904-915, August 1994.

[3] A. Pries, T. Secomb, "Microvascular blood viscosity in vivo and the endothelial surface layer," *Am J Physiol Heart Circ Physiol*, vol. 289, pp. H2657-H2664, July 2005.